Geophys. J. Int. (2000) **140,** 63–70

Body wave moment tensor inversion of local earthquakes: an application to the South Iceland Seismic Zone

Z. Hossein Shomali and Ragnar Slunga

Department of Earth Sciences, Uppsala University, Villvagen 16, *Uppsala* S-752 36, *Sweden. E-mail: hs@geofys.uu.se; ragnar@geofys.uu.se*

Accepted 1999 July 30. Received 1999 June 30; in original form 1998 May 18

SUMMARY

The focal mechanisms and scalar seismic moments of four local earthquakes are determined using a seismic moment inversion method for frequencies larger than those of dominant oceanic noise and lower than the corner frequency. The earthquakes have epicentral distances ranging from 9 to 42 km and were recorded by the South Iceland Lowland (SIL) seismic network. Synthetic seismograms are computed using the frequency–wavenumber integration technique for an elastic horizontally layered medium. Moment tensor inversion is then carried out using windows designed around *P* and *S* waveforms on individual components and at individual seismic stations. The waveforms within each window are then inverted in the time domain simultaneously on all components and at all available seismic stations. The trace elements of the seismic moment tensor are subject to the deviatoric constraint (zero trace element). The results of the inversion are classified as a sum of double couple and CLVD sources, and then compared with the results from the automatic amplitude spectra method routinely used in the SIL network. The comparison shows fairly good agreement between the two approaches, considering that the former uses both amplitude and phase information and the latter uses only amplitude information. The first three events studied have moment magnitudes in the range $2.3 \leq M_w \leq 3.1$ and comprise two foreshocks and an associated main shock. The weighted least squares inversions for these events show dominant strike slip faulting with scalar seismic moments of the order of $0.285 \times 10^{13} \leq M_0 \leq 4.966 \times 10^{13}$ N m. The fourth event is characterized by a moment magnitude $M_w = 2.2$ and scalar seismic moment $M_0 = 0.243 \times 10^{13}$ N m. This event also shows a significant strike slip component.

Key words: radiation patterns, seismic moment tensor, South Iceland Seismic Zone.

INTRODUCTION

The seismic moment inversion method is widely employed in determining the focal mechanism of earthquakes. This method can be applied to a variety of categories of waves, for example free oscillations (e.g. Gilbert & Dziewonski 1975), surface waves (e.g. Romanowicz 1981), long-period body waves (e.g. Langston 1981; Wallace & Helmberger 1982) and short-period body waves (e.g. Saikia & Herrmann 1985; Saikia 1986; Saikia & Herrmann 1986; Ebel & Bonjer 1990; Koch 1991). A moment tensor inversion can be manipulated either in the time domain (e.g. Langston 1981) or the frequency domain (e.g. Romanowicz 1981), and a single station is often sufficient for the recovery of a focal mechanism (e.g. Langston 1981; Dreger & Helmberger 1991).

In this paper, focal mechanisms and scalar seismic moments are first determined for four local earthquakes recorded by the SIL (South Iceland Lowland) network. The results are then compared with those routinely produced by the SIL network using a spectral amplitude method (Rögnvaldsson & Slunga 1993). The spectral amplitude method is based on a ray theory algorithm valid for far-field data and requires very little computation. The moment tensor inversion is applied to short-period body wave data. The most time-consuming part of performing a successful moment tensor inversion is the computation of the Green's function. Prior to analysis, the observed displacement data are bandpass filtered for frequencies above the dominant oceanic noise and below the corner frequency. This is done to remove low-frequency external noise and because structural details about which we know little can strongly affect higher frequencies.

In this study, five three-component seismic stations were used to analyse each event (Table 1).

Table 1. Seismic stations used in the inversion.*

Station	Latitude (°N)	Longitude (°E)	Elevation (km)
ASM	63.834	−20.615	0.019
BJA	63.946	−21.303	0.058
HAU	63.969	−19.965	0.099
HEI	64.200	−21.237	0.160
SAU	63.990	−20.416	0.077
SOL	63.929	−20.944	0.031

*Data from the SIL network.

THE EARTHQUAKE DATA SET

The extended SIL data acquisition system consists of 27 remote seismic stations connected through an X.25 link to a common data centre. Each station is equipped with a three-component seismometer with an eigenfrequency of 0.2 or 1 Hz (negative feedback Lennartz sensor), a 16-bit gain-ranging digitizer with an Omega synchronized clock, and a 32-bit computer (PC) running the UNIX operating system. The data are initially filtered and decimated down to 100 samples per second. The dynamic range of the system is 136 dB and the resolution is 3.67 nm s^{-1}. The velocity response of the system is flat between the seismometer eigenfrequency and 34 Hz (Bödvarsson *et al.* 1996). Earthquakes within the SIL area down to a magnitude $M_L = -0.5$ are selected and located, and magnitudes and focal mechanisms are estimated automatically by the network (Stefánsson *et al.* 1993). The estimated absolute depth uncertainties for single and multi-event locations are typically 1 km and 100–200 m, respectively. The relative location accuracy for multi-event location is approximately 10 m (Slunga *et al.* 1995).

The first three earthquakes analysed ($M_w = 2.3$–3.1) were chosen from an extensive earthquake swarm at the western end of the South Iceland Seismic Zone (SISZ) from 1994 August 13 to 1994 August 21. More than 3000 earthquakes were recorded in that period, and on August 19 more than 600 earthquakes were recorded in one day. The fourth earthquake ($M_w = 2.2$) occurred in central South Iceland on 1996 March 17. The events and seismic stations used are depicted in Fig. 1, and the source parameters of the events are summarized in Table 2.

WAVEFORM MODELLING

The frequency–wavenumber (F–K) integration method (Bouchon 1981 and Saikia 1994) was employed to compute the complex spectra of the eight Green's function components associated with three fundamental faults caused by an arbitrary shear dislocation point source in a plane layered elastic medium. The Fourier transform of the observed displacements at the free surface of the Earth in a cylindrical coordinate system is defined as (Herrmann & Wang 1985 and Jost & Herrmann 1989)

$$\begin{aligned} w(r, 0, \omega) &= Z_{SS} A_1 + Z_{DS} A_2 + Z_{DD} A_3 , \\ q(r, 0, \omega) &= R_{SS} A_1 + R_{DS} A_2 + R_{DD} A_3 , \\ v(r, 0, \omega) &= T_{SS} A_4 + T_{DS} A_5 , \end{aligned} \tag{1}$$

where w, q and v are the vertical, radial and tangential displacements, respectively, or the components of the synthetic seismograms, and r denotes the epicentral distance. The functions Z_{ii}, R_{ii} and T_{ii} are the components of the Green's function required to evaluate a whole waveform excited by a double-couple source (the isotropic components of the Green's function are ignored). The subscripts 'SS', 'DS' and 'DD' are the three fundamental faults: vertical strike slip, vertical dip slip and 45°-dipping dip slip, respectively. The coefficients A_i are the azimuthal radiation patterns of the waveform for a double couple source and are defined as

$$\begin{aligned} A_1 &= 1/2(M_{xx} - M_{yy}) \cos 2\Phi + M_{xy} \sin 2\Phi , \\ A_2 &= M_{xz} \cos \Phi + M_{yz} \sin \Phi , \\ A_3 &= -1/2(M_{xx} + M_{yy}) , \\ A_4 &= 1/2(M_{xx} - M_{yy}) \sin 2\Phi - M_{xy} \cos 2\Phi , \\ A_5 &= -M_{yz} \cos \Phi + M_{xz} \cos \Phi . \end{aligned} \tag{2}$$

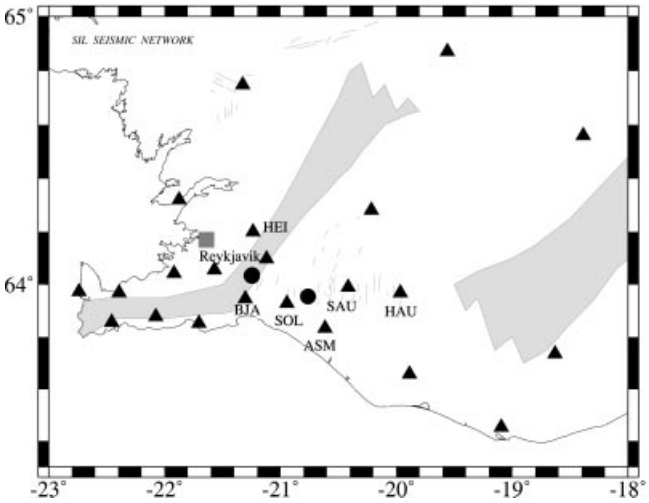

Figure 1. Epicentral map of the events studied (circles), within the SIL seismic network. The first three events are close together and are shown by one circle. The SIL seismic stations are shown as triangles—only those used in the present study are named. The shaded areas show volcanic zones, and the thin lines denote the active faults.

Table 2. Source parameters of the studied events, calculated by the spectral amplitude method.*

Event	Date yymmdd	Origin Time (UTC)	Latitude (°N)	Longitude (°E)	Depth** (km)	M_0 (N m)	M_L	$\langle r \rangle$ (m)	$\langle \Delta\sigma \rangle$ (Mpa)	$\langle s \rangle$ (mm)
1	940819	191636.7	64.037	−21.244	1.0(1.6)	0.972×10^{13}	3.0	255	0.25	4.2
2	940819	191804.9	64.033	−21.245	2.6(1.6)	0.898×10^{13}	3.0	255	0.24	2.6
3	940819	191841.6	64.034	−21.250	1.5(1.6)	9.240×10^{13}	3.8	287	1.70	26.8
4	960317	035627.6	63.955	−20.762	4.4(–)	0.344×10^{13}	2.5	153	0.42	2.2

*Data from the SIL network. **Determined by multi-event location (Slunga *et al.* 1995). The symbols are: M_0, scalar seismic moment; M_L, local magnitude; $\langle r \rangle$, average fault radius; $\langle \Delta s \rangle$, average stress drop; $\langle s \rangle$, average peak slip on the fault plane.

In this notation, Φ is the forward azimuth and M_{ij} are the components of the seismic moment tensor. M_{ij} are frequency-dependent and related to the orientation of the fault and auxiliary planes for double couple sources as follows (Aki & Richards 1980):

$$\begin{aligned}
M_{xx} &= -M_0(\sin\delta\cos\lambda\sin 2\varphi + \sin 2\delta\sin\lambda\sin^2\varphi),\\
M_{xy} &= M_0(\sin\delta\cos\lambda\cos 2\varphi + (1/2)\sin 2\delta\sin\lambda\sin 2\varphi)\\
&= M_{yx},\\
M_{xz} &= -M_0(\cos\delta\cos\lambda\cos\varphi + \cos 2\delta\sin\lambda\sin\varphi) = M_{zx},\\
M_{yy} &= M_0(\sin\delta\cos\lambda\sin 2\varphi - \sin 2\delta\sin\lambda\cos^2\varphi),\\
M_{yz} &= -M_0(\cos\delta\cos\lambda\sin\varphi - \cos 2\delta\sin\lambda\cos\varphi) = M_{zy},\\
M_{zz} &= M_0\sin 2\delta\sin\lambda,
\end{aligned} \tag{3}$$

where φ, δ and λ are the strike, dip and rake of the fault planes and M_0 is the scalar seismic moment.

The linear relations between the observed displacements and the seismic moment tensor for a known source time function are obtained by substituting eq. (2) into eq. (1). The result can be written in the following matrix form for N observational data points (representation theorem, Aki & Richards 1980):

$$\mathbf{U}(w, q, v, \omega) = \mathbf{GM}. \tag{4}$$

The vector $\mathbf{U}$, with dimension $(N \times 1)$, is composed of the Fourier transformations of the observed displacements and contains all the components of ground displacements at the seismic stations. The $(N \times 5)$ matrix $\mathbf{G}$ is composed of the Green's function components. $\mathbf{M}$ is a (5×1) vector consisting of the five moment tensor components.

The components of the Green's function are calculated at each epicentral distance and assumed depth, based on the frequency-domain algorithm given by Saikia (1994). The evaluated complex spectra of the Green's function components are transformed into the time domain by inverse transformation. A system of linear equations is then formed in order to perform the inversion (eq. 4 in the time domain). The source time function is assumed to be a Heaviside function. This means that the moment tensor components in eq. (4) become scalars and thus a convolution operator is no longer needed to evaluate the synthetic seismograms in the time domain.

INVERSION

Inversion was performed in two steps. In the first step, the system of linear equations introduced in eq. (4) was solved by imposing the deviatoric constraint, $M_{zz} = -(M_{xx} + M_{yy})$, to the trace elements of the seismic moment tensor. This constraint implies that the source has no volumetric component. The dominance of the shear-slip mechanism in the events studied has been reported previously (Slunga *et al.* 1995). Thus, the number of unknown model parameters is reduced to the five components of the seismic moment tensor. By using more independent observed data, the above linear system becomes overdetermined and can be solved according to a weighted least squares approach. The use of stations at many different distance ranges can lead to significant differences in individual station variances, which can give artificial weight to the closest stations in the inversion. Because body waves decay roughly as the reciprocal of distance travelled, the differences between the observed and predicted data were weighted in proportion to distance (Dreger & Langston 1995).

In the second step, the fault plane orientations and scalar seismic moment were determined based on the system of equations defined in eq. (3) by performing an inversion for strike, dip, rake and scalar seismic moment. The alternative approach, estimating the fault plane orientation and scalar seismic moment directly from the observed waveform data, requires non-linear inversion. It should be noted that the algorithm presented here, eqs (1)–(3), is more useful for calculating the fault parameters (strike, dip and rake) than the moment tensor components. The automatic spectral amplitude method used by the SIL network determines source parameters of earthquakes in the form of fault parameters. Therefore in order to make a comparison between these parameters and the current research, the algorithm given was followed in waveform modelling.

Regarding eq. (2), the coefficient A_3 is most directly constrained by the deviatoric constraint. Thus the coefficient is poorly determined for a source with a significant volumetric component. The contribution of this coefficient is to the vertical and radial components (eq. 1). Therefore, the degree of similarity between the observed data and corresponding synthetics is more sensitive for the vertical and radial components than for tangential components, as the volumetric component of a source varies while calculating the synthetics.

A windowing method was used for the moment tensor inversion. Around each *P* and *S* waveform on each component at the individual seismic stations, Hanning windows were designed (the windows may contain some of the converted phases too). The moment tensor inversion was then performed inside each window simultaneously for all components at the individual seismic stations. The inversion was optimized by applying a cross-correlation routine to align the synthetic seismograms with the observed data. Three fundamental fault Green's functions for each component were correlated with the respective data and the best correlation was used to determine the zero time offset for all three components (Dreger & Langston 1995). This alignment is necessary to compensate for uncertainties in the structural velocity model used, errors in the estimation of epicentral distances and other relevant sources of error, and was done before the mechanism had been estimated. According to this algorithm, it is assumed that the best solution is the solution that has the maximum variance reduction. The inversion was done for three groups of data sets. First *P* and *S* waveforms were inverted separately, and then *P* and *S* waveforms were inverted simultaneously. Finally, the results of the inversion were classified as a sum of double couple and CLVD sources. Error estimations of the solutions are not carried out in this study.

PREPARATION OF THE DATA SET

In this section, the steps used to prepare the data are described. First, the horizontal components of the observed data were rotated about the source–receiver backazimuth to form the radial and tangential components. In Fig. 2, the waveforms of event number 3 at the five seismic stations used are shown for the rotated and vertical components. Second, the effect of the instrument response was removed in order to transform the observed data into proportional ground motion displacement. Third, the observed data were filtered using a two-pole

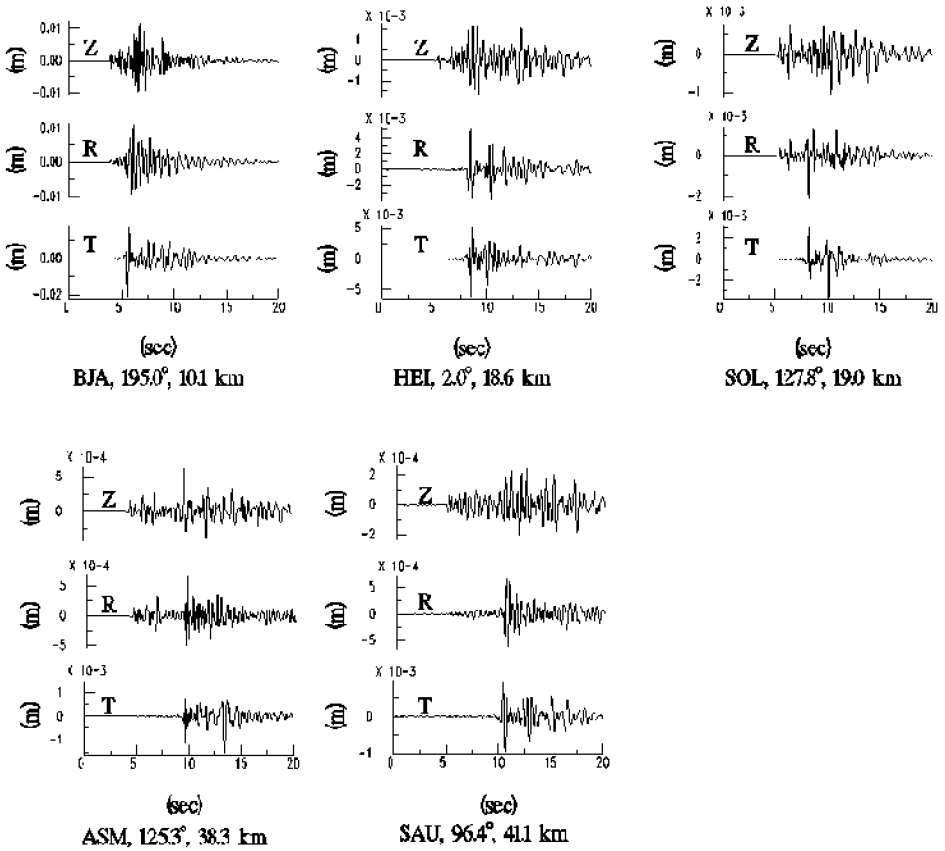

Figure 2. Displacement seismograms of event 3 at the five seismic stations used. Z, R and T stand for vertical, radial and tangential components, respectively. Starting times are arbitrary. The numbers next to the station names are the station azimuth (°) and epicentral distance (km). The seismic stations are shown in order of increasing epicentral distance.

Butterworth filter. The filter was applied forwards and backwards in order to eliminate the phase distortion. Naturally, this violates causality (Plešinger *et al.* 1996). The lower corner frequency of the filter was fixed above the dominant oceanic noise, and the upper corner of the filter was taken below the corner frequencies of the data. This allows a Heaviside function to be used as a source time function in the calculations. For events 1–3, two-pole Butterworth filters with corners at 1 and 4 Hz were applied, and for event 4 the corners were at 1 and 6 Hz. The same filters were applied to the corresponding synthetic seismograms.

Data processing was performed using the SAC[1] (Seismic Analysis Code, Lawrence Livermore National Laboratory) package.

RESULTS OF THE WAVEFORM MODELLING

The structural model used to generate the required Green's functions is shown in Table 3. The near-surface layer velocities were obtained after a number of trials in order to produce a reasonable match between the observed waveforms and corresponding synthetics. Note that, except for the first layer, the quality factors of the P waves (Q_P) are less than those for the S waves (Q_S), as is routinely the case in the SIL network.

[1] The package is available at the following electronic address: http://www-ep.es.llnl.gov/tvp/sac.html#Availability

Table 3. Structural model used.*

Depth (km)	P velocity (km s^{-1})	S velocity (km s^{-1})	Density (g cm^{-3})	Q_P	Q_S
0.0	3.00	1.69	2.6	100.0	100.0
1.0	3.50	2.00	2.6	450.0	900.0
2.0	5.16	2.90	2.9	450.0	900.0
3.0	5.60	3.15	2.9	450.0	900.0
4.0	5.96	3.35	2.9	450.0	900.0
6.0	6.50	3.65	2.95	450.0	900.0
9.0	6.73	3.78	3.0	450.0	900.0
20.0	7.20	4.04	3.3	450.0	900.0

*A linear interpolation for velocity, density and quality factor is assumed. The S wave velocities are set to $V_P/\sqrt{3}$.

In this study, P and SV waves on the vertical and radial components and SH waves on the tangential component were used in the waveform modelling. The S waveform is usually the dominant phase for the events studied, and, excluding the nodal seismic station, the fit between the observed data and synthetics was mainly controlled by them. Generally, the waveform fit is much better for the tangential components than for the other components, and the vertical components show a better fit than the radial components. As mentioned earlier, the inversion was carried out separately for P, S, and P and S waveforms. The inversion for the P waveforms did not converge. This may relate to the signal-to-noise ratio or the high

amount of *P* to *S* conversion for the events studied. The inversions based on *S*, and *P* and *S* waveforms produced almost the same results. Throughout this study, the fault plane solutions based on the inversion of the *P* and *S* waveforms together are considered to be the more reliable solutions, because more constraints are imposed.

Events 1 and 2 are considered as foreshocks of event 3. For events 1 and 3, stations BJA, HEI, SOL, ASM and SAU were used in the inversion, and for event 2 station SAU was replaced by HAU. The Green's functions were calculated at depths of 1.0, 1.6, 2.0, 2.5 and 3.0 km for each station. The depth of 1.6 km comes from the multi-event location (Slunga *et al.* 1995), and was found to produce a good fit between the observed data and synthetics. The window lengths used for inverting the data, including *P* and *S* waves, varied from 1.5 to 2.0 s. The results of the inversion are shown in Table 4, and the *P* and *S* inversions are illustrated in Figs 3 and 4, for events 1 and 3. The fault plane solutions based on the automatic spectral amplitude method (Rögnvaldsson & Slunga 1993), which is routinely used in the SIL network, are listed in Table 5. The spectral amplitude method is based on a ray theory algorithm, giving simple Green's functions (delayed impulse pulses) for the far-field waves. Therefore from Tables 4 and 5 one can compare the results from the waveform inversion based on both amplitude and phase information, and the automatic spectral amplitude method using only amplitude information.

For event 1, the fault plane solution from this study appears to be better than the corresponding orientation from the routine SIL analysis, if it is assumed that events 1–3 occurred on the same plane, a hypothesis supported by results from the multi-event location method (Slunga *et al.* 1995).

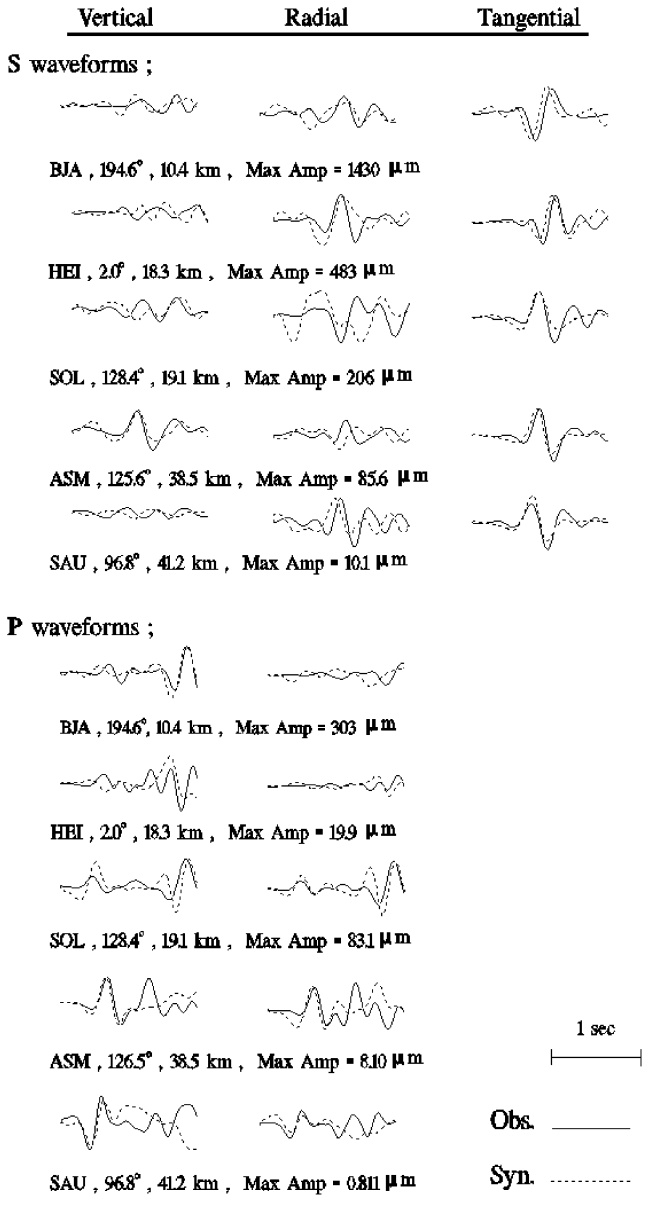

Figure 3. Moment tensor inversion results for event 1 for the *P* and *S* waveform inversion. The solid lines are the observed data, and the dashed lines are synthetics. The numbers beneath each waveform refer to the station azimuth (°) and epicentral distance (km). Windows specifications are given in the text.

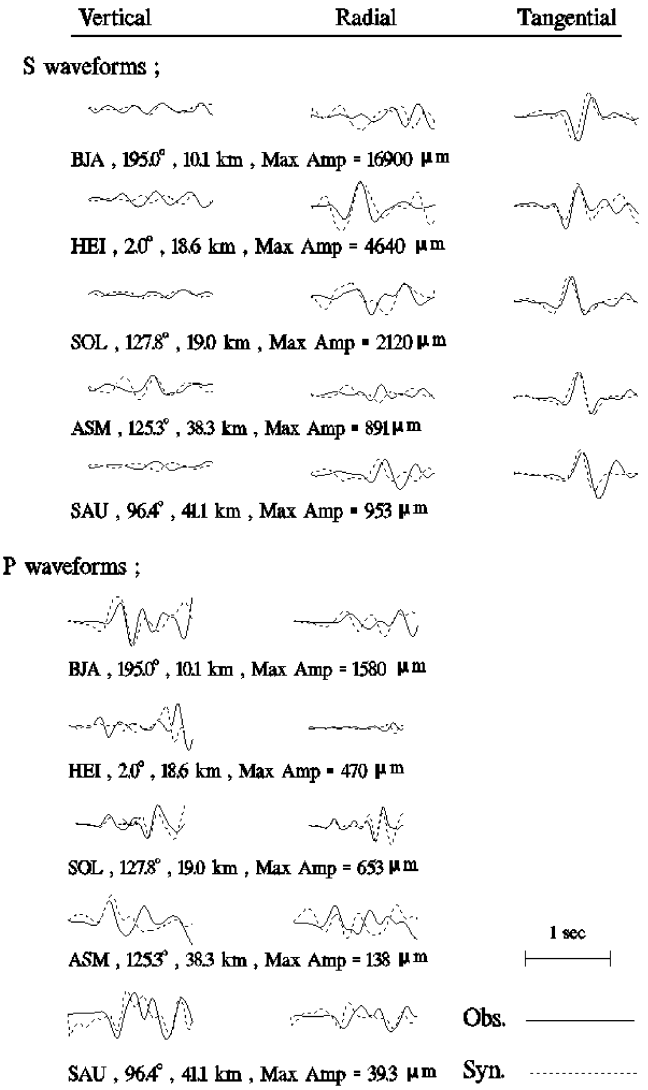

Figure 4. Moment tensor inversion result for event 3 for the *P* and *S* waveform inversion (for other parameters see the caption of Fig. 3).

Table 4. Results of the inversion.

	S wave inversion results				*P* and *S* wave inversion results			
	Event no. 1	Event no. 2	Event no. 3	Event no. 4	Event no. 1	Event no. 2	Event no. 3	Event no. 4
M_{xx}*	0.333	0.215	2.777	0.075	0.178	0.216	2.715	0.019
M_{xy}	−0.184	−0.385	−3.251	−0.241	0.138	−0.374	−3.241	−0.186
M_{xz}	−0.204	−0.109	−1.882	−0.138	−0.175	−0.105	−1.875	−0.109
M_{yy}	−0.405	−0.138	−3.329	−0.099	−0.181	−0.138	−3.260	−0.108
M_{yz}	0.061	0.019	−1.638	−0.063	−0.027	0.025	−1.460	−0.032
M_0	0.468	0.436	5.051	0.296	0.285	0.425	4.966	0.243
M_W	2.4	2.4	3.1	2.3	2.3	2.4	3.1	2.2
Strike (φ°)	208, 305	282, 192	112, 203	101, 191	296, 203	283, 192	112, 203	105, 195
Dip (δ°)	72, 70	88, 77	88, 63	89, 60	85, 54	87, 78	89, 63	90, 62
Slip (λ°)	159, 19	13, 178	−27, −178	−30, −179	36, 174	12, 177	−27, −179	−28, −179
Depth (km)	1.6	1.6	1.6	4.4	1.6	1.6	1.6	4.4
Double-Couple %	85	63	62	70	68	61	66	99
CLVD %	15	37	38	30	32	39	34	1

*All moments are in units of 10^{13} N m.

Table 5. Spectral amplitude results from routine analysis carried out by the SIL network.

	Event no. 1	Event no. 2	Event no. 3	Event no. 4
Strike (φ°)	300, 31	302, 206	97, 201	77, 189
Dip (δ°)	73, 89	70, 76	79, 39	55, 62
Slip (λ°)	−1, −163	15, 159	−53, −162	−35, −139
Depth (km)	1.0 ± 2.3	2.6 ± 3.7	1.5 ± 1.9	4.4 ± 1.5

For event 4, synthetic seismograms were evaluated at depths of 2.0, 3.0 and 4.5 km at each seismic station (SOL, ASM, SAU, BJA and HEI). The depth of 4.5 km was found to produce a good match between the observed data and the synthetics. For this event, a window of 1.5 s containing both *P* and *S* waveforms was used in the inversion. The results of the inversions are tabulated in Table 4, and the results for the inversion of the *P* and *S* waveforms are shown in Fig. 5. The results obtained agree well with those from the previous analysis (Tables 4 and 5).

From Table 4 it can also be seen that the inversion based on the *S* waveforms can determine the fault plane orientation and scalar seismic moment well. The inclusion of more constraints imposed by the *P* waveforms causes some slight changes in the orientation of the estimated fault planes and decreases the estimated values of the scalar seismic moment. The estimated values of scalar seismic moment in Table 4 are less than those calculated by the routine spectral amplitude method (Tables 2 and 4). It has been reported (Haar *et al.* 1984) that scalar seismic moments estimated using time domain methods are lower than those determined by frequency domain techniques. This is partly because in the time domain method both amplitude and phase information is used. Furthermore, it has been suggested that instrument effects may cause slight differences in determining the scalar seismic moment (Saikia & Herrmann 1986). The relatively high percentage of the CLVD sources may in some cases be attributed to poor structural models of the complex tectonic characteristics of the area studied.

Figs 3, 4 and 5 illustrate that the waveform inversion can provide a reasonable representation of the major features of

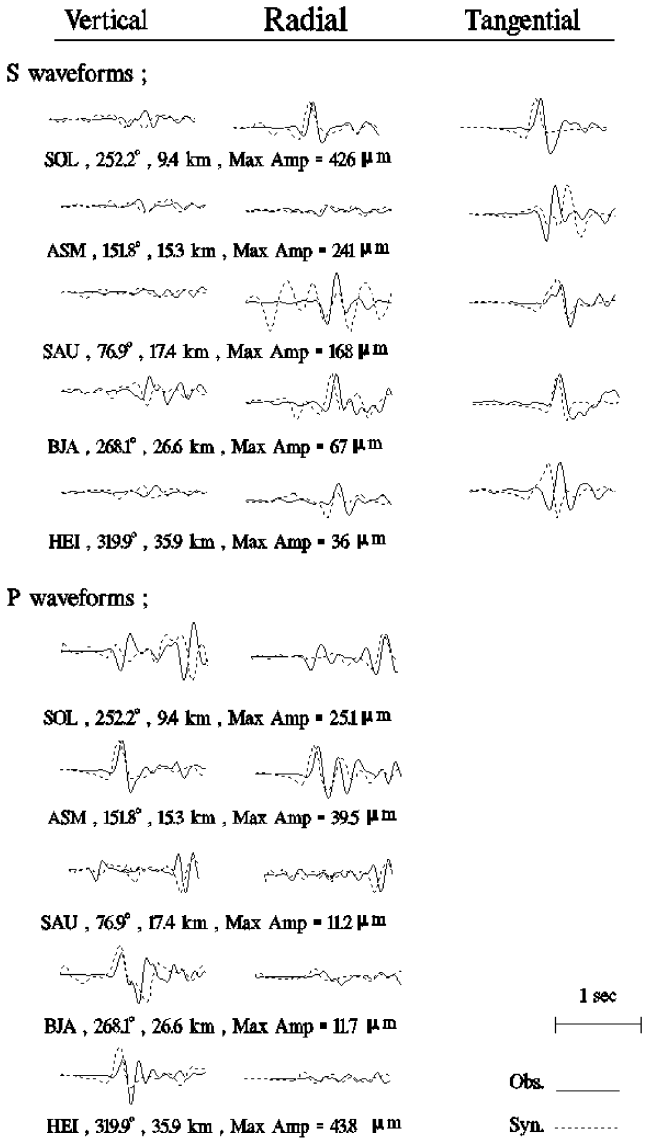

Figure 5. Moment tensor inversion result for event 4 for the *P* and *S* waveform inversion (for other parameters see the caption of Fig. 3).

the observed data. The matching between observed data and associated synthetics is dominated by the *SH* waves (tangential components). In Fig. 6, the focal mechanisms of *P* waves obtained from the current study are compared with those estimated using the spectral amplitude method.

DISCUSSION AND CONCLUSIONS

The focal mechanisms and scalar seismic moments of four local earthquakes in South Iceland were determined using seismic moment inversion of short-period body waves. A weighted least squares inversion method was used to invert the observed waveforms, and the results were presented as a sum of double couple and CLVD sources. Good agreement between the waveform modelling and the results based on the ray theory routinely carried out in the SIL network was achieved. The inversion algorithm could determine the fault plane orientation and scalar seismic moment correctly, even under conditions of poor azimuthal coverage (events 1–3).

The fit between the observed data and synthetics for the vertical and radial components (*P* and *S* waves) varied from case to case, but in general the misfit for the *SH* waves was small. A comparison of the amplitude and duration of *SH* waves (as a dominant phase) on the observed data and corresponding synthetics implies that the type of source time function chosen was suitable. The inversion based on *S* waveforms could predict the synthetics well. The addition of *P* waveforms while inverting the data lowered the estimated values of the scalar seismic moments. Inversion using *P* waveforms only did not converge, probably because of the lower signal-to-noise ratio or high amount of *P* to *S* conversion. The estimated values of the scalar seismic moments from the current study are lower than those calculated by the spectral amplitude method. The observed mismatch between some of the observed and synthetic waveforms on some components and the relatively high percentage of CLVD sources in some cases occur because of the approximation to the Green's function in such a tectonically complex area.

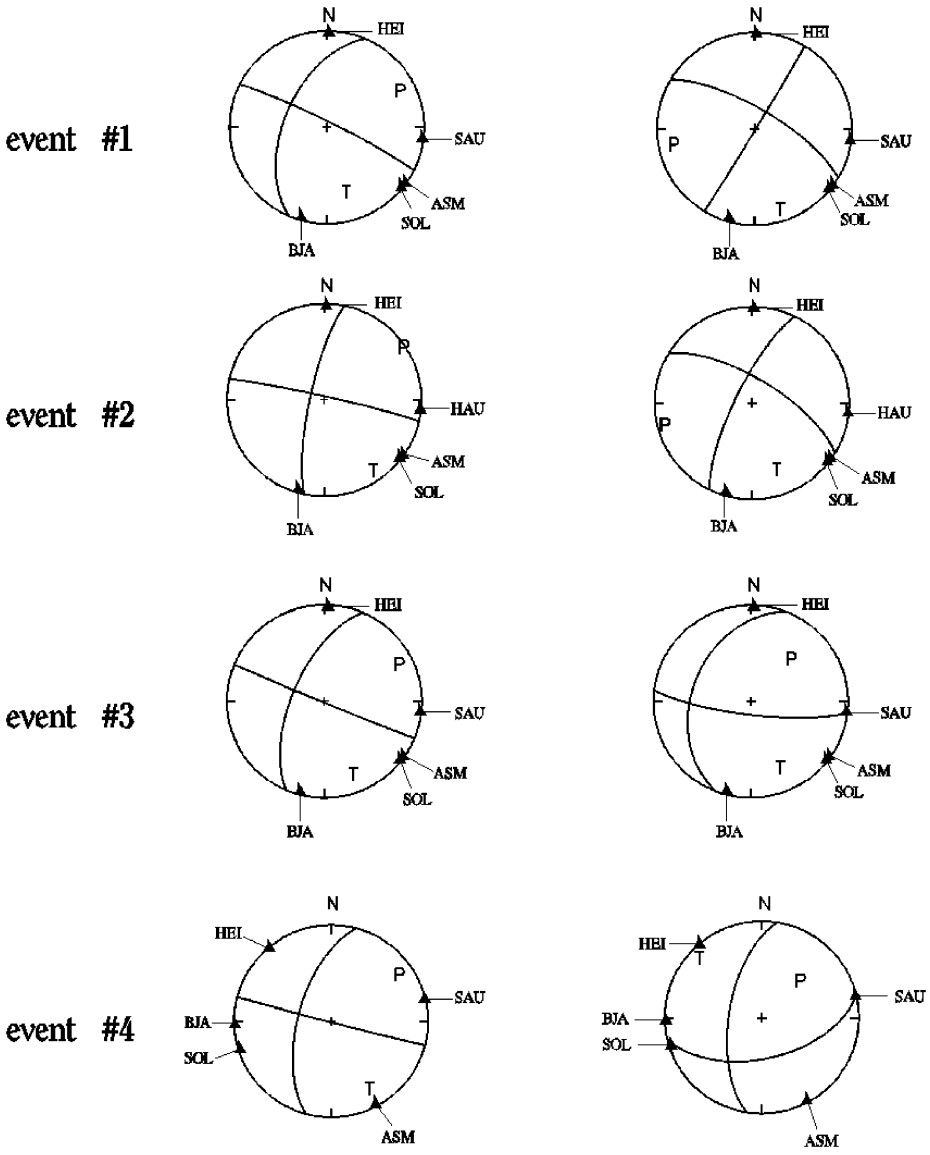

Figure 6. *P*-wave focal mechanisms obtained from the current research (left column) and those from the spectral amplitude method routinely used in the SIL network (right column). Stations used are shown by triangles.

ACKNOWLEDGMENTS

This work was supported by the Swedish Natural Science Research Council (NFR). The software was provided by the Incorporated Research Institution for Seismology (IRIS). The comments of R. Roberts, O. Kulhánek and R. Bödvarsson were much appreciated.

REFERENCES

Aki, K. & Richards, P.G., 1980. *Quantitative Seismology: Theory and Methods,* Vol. I, W. H. Freeman, San Francisco.

Bödvarsson, R., Rögnvaldsson, S.Th., Jakobsdóttir, S.S., Slunga, R. & Stefánsson, R., 1996. The SIL data acquisition and monitoring system, *Seism. Res. Lett.,* **67,** 35–46.

Bouchon, M., 1981. A simple method to calculate Green's functions for elastic layered media, *Bull. seism. Soc. Am.,* **71,** 959–971.

Dreger, D.S. & Helmberger, D.V., 1991. Complex faulting deduced from broadband modeling of the 28 February 1990 Upland earthquake ($M_L = 5.2$), *Bull. seism. Soc. Am.,* **81,** 1129–1144.

Dreger, D.S. & Langston, C., 1995. *Moment Tensor Inversion Workshop,* Incorporated Research Institutions for Seismology, Data Management Center, Seattle.

Ebel, J.E. & Bonjer, K.-P., 1990. Moment tensor inversion of small earthquakes in southwestern Germany for the fault plane solution, *Geophys. J. Int.,* **101,** 133–146.

Gilbert, F. & Dziewonski, A.M., 1975. An application of normal mode theory to the retrieval of structural parameters and source mechanisms from seismic spectra, *Phil. Trans. R. Soc. Lond.,* A, **278,** 187–269.

Haar, L., Fletcher, J.B. & Mueller, C.S., 1984. The 1982 Enola, Arkansas, swarm and scaling of ground motion in the eastern United States, *Bull. seism. Soc. Am.,* **74,** 2463–2482.

Herrmann, R.B. & Wang, C.Y., 1985. A comparison of synthetic seismograms, *Bull. seism. Soc. Am.,* **75,** 41–56.

Jost, M.L. & Herrmann, R.B., 1989. A student's guide to and review of moment tensors, *Seism. Res. Lett.,* **60,** 37–57.

Koch, K., 1991. Moment tensor inversion of local earthquake data—II. Application to aftershocks of the May 1980 Mammoth lakes earthquakes, *Geophys. J. Int.,* **106,** 321–332.

Langston, C.A., 1981. Source inversion of seismic waveforms: The Koyna, India, earthquakes of 13 September, 1967, *Bull. seism. Soc. Am.,* **71,** 1–24.

Plešinger, A., Zmeškal, M. & Zedník, J., 1996. *Automated Preprocessing of Digital Seismograms: Principles and Software,* Version 2.2, ed. Bergman, E., Prague.

Rögnvaldsson, S.Th. & Slunga, R., 1993. Routine fault plane solutions for local networks: a test with synthetic data, *Bull. seism. Soc. Am.,* **83,** 1232–1247.

Romanowicz, B., 1981. Depth resolution of earthquakes in central Asia by moment tensor inversion of long-period Rayleigh waves: Effects of phase velocity variations across Eurasia and their calibration, *J. geophys. Res.,* **86,** 5963–5984.

Saikia, C.K., 1986. Waveform modeling of two earthquakes ($M \approx 1.1$) of July 1983 from the Miramichi aftershock zone, *Bull. seism. Soc. Am.,* **76,** 725–732.

Saikia, C.K. & Herrmann, R.B., 1985. Application of waveform modeling to determine focal mechanisms of four 1982 Miramichi aftershocks, *Bull. seism. Soc. Am.,* **75,** 1021–1040.

Saikia, C.K. & Herrmann, R.B., 1986. Moment-tensor solutions for three 1982 Arkansas swarm earthquakes by waveform modeling, *Bull. seism. Soc. Am.,* **76,** 709–723.

Saikia, C.K., 1994. Modified frequency–wavenumber algorithm for regional seismograms using Filon's quadrature: modelling of Lg waves in eastern North America, *Geophys. J. Int.,* **118,** 142–158.

Slunga, R., Rögnvaldsson, S.Th. & Bödvasrsson, R., 1995. Absolute and relative locations of similar events with application to micro-earthquakes in southern Iceland, *Geophys. J. Int.,* **123,** 409–419.

Stefánsson, R., Bödvarsson, R., Slunga, R., Einarsson, P., Jakobsdóttir, S., Bungum, H., Gregersen, S., Havskov, J., Hjelme, J. & Korhonen, H., 1993. Earthquake prediction research in the South Iceland Seismic Zone and the SIL project, *Bull. seism. Soc. Am.,* **83,** 696–716.

Wallace, T.C. & Helmberger, D.V., 1982. Determining source parameters of moderate size earthquakes from regional waveforms, *Phys. Earth planet. Inter.,* **30,** 185–196.